Exploring Airfoil Tonal Noise Reduction with Elastic Panel Using Perturbation Evolution Method

I. Arif*, Di. Wu† Garret C. Y. Lam‡ and Randolph C. K. Leung§
The Hong Kong Polytechnic University, Hung Hum, Kowloon, Hong Kong, People's Republic of China.

Nomenclature

AoA	=	angle of attack
a	=	speed of sound
C	=	panel structural damping coefficient
c	=	airfoil chord
D	=	panel bending stiffness
E	=	energy
$\boldsymbol{F}, \boldsymbol{F_v}, \boldsymbol{G}, \boldsymbol{G_v}, \boldsymbol{U}$	=	flow flux conservation variables
$(f_{bl})_n$	=	n^{th} harmonic of natural boundary layer instability
$(f_{EP})_n$	=	n^{th} natural frequency of panel vibration mode
$f_{exc,n}$	=	frequency of acoustic excitation
h	=	panel thickness
K	=	stiffness of foundation supporting panel
L	=	panel length
N	=	panel internal tensile stress
n	=	mode number
p	=	pressure
p_{ex}	=	net pressure exerted on panel surface
q_x, q_y	=	heat flux
Re_c	=	Reynolds number based on airfoil chord
SPL	=	sound pressure level
T	=	panel external tension
t	=	time
u, v	=	velocity components along streamwise and transverse directions

*PhD Student, Department of Mechanical Engineering; irsalan.arif@connect.polyu.hk.
†PhD Student, Department of Mechanical Engineering; 13903590r@connect.polyu.hk.
‡Research Fellow, Department of Mechanical Engineering; garret.lam.hk@connect.polyu.hk.
§Associate Professor, Department of Mechanical Engineering; mmrleung@polyu.edu.hk, and Senior Member AIAA.

w = panel vibration displacement

ρ = density

τ_{xx}, τ_{xy}, τ_{yy} = flow shear stresses

ϕ_n = phase of acoustic excitation

Superscript

$'$ = perturbation

$\hat{}$ = complex amplitude

Subscript

0 = freestream condition

$base$ = base flow

NR = non-resonant panel

R = resonant panel

rms = root mean square value

I. Introduction

Airfoil tonal noise is a popular problem with many flight vehicles and flow-moving devices operating at low Reynolds number, where it manifests itself as prominent discrete tones in the sound pressure spectrum approximately tens of dB above the background noise. Brooks et al. [1] gave a classification of the different flow physical mechanisms that can lead to noise radiation from airfoil. Usually when considering tonal noise of low Reynolds number airfoil flow, most studies focus upon trailing edge noise which arises from a complex interaction between boundary-layer instabilities on the airfoil surfaces and the acoustic pressure field generated by the flow. A resonant aeroacoustic feedback loop mechanism is usually in place for the production of discrete tones. The study of airfoil tonal noise is still of high importance. Tonal noise is commonly observed in acoustic signatures of small aircraft, low-speed rotors, fans, ventilators, and wind-turbine blades. Due to the increasingly frequent operations of micro air vehicles and the unmanned air vehicles in close proximity to people, interest in research on the airfoil tonal noise has been on the rise during recent years. These vehicles are commonly propelled with efficient electric motors and the tonal noise from their wings starts to emerge as a major contributor to the overall noise radiation. Therefore, in a military context, low or suppressed noise radiation from wings is imperative in vehicle design, which helps increase the survivability of the vehicle during operation. On the other hand, for many civil goals, these vehicles are popularly used for such purposes as aerial searching, film making, law enforcement, etc. The low noise performance would enlarge the possible range of

missions and minimize acoustic nuisance to the environment.

In past decades many studies have been devoted to achieve a good understanding of the physical mechanisms of airfoil tonal noise generation. An early detailed experimental study with NACA 0012 and NACA 0018 airfoils in low turbulence and open-jet wind tunnel were carried out by Paterson et al. [2]. Their results showed that in general the frequency of dominant acoustic radiation appeared to scale up with the fifth order of free-stream velocity. In addition, their most significant finding was the discovery of ladder-like structure of the radiated discrete tones and the frequency of each ladder dependence on the free-stream velocity with an exponent of 0.8. Paterson et al. [2] attributed this phenomenon as a result of the noise generation associated with the vortex shedding process in airfoil wake. Tam [3] gave an alternative view to Paterson et al's observation and proposed a model involving a self-excited feedback loop that is responsible for the tonal noise generation. He thought the flow disturbances are generated near the airfoil trailing edge due to the upstream traveling acoustic wave. These disturbances then amplified in the wake and resulted in acoustic generation. Part of the generated acoustic wave propagated to the airfoil trailing edge, which promotes the injection of disturbances there and closes the feedback loop. Subsequent study by Arbey et al. [4] provided further support to Tam's model. They confirmed the source of the noise was very close to the trailing edge and the feedback loop actually occurs between the maximum velocity point on the airfoil suction side and the trailing edge. Since then, there are many experimental and computational studies devoted along this line of thought. Desquesnes et al. [5] carried out the first numerical study of the airfoil tonal noise generation and suggested that the feedback loop might occur on the airfoil suction and pressure side simultaneously and cross-talk between the loops on both sides is possible. This idea was further analyzed with extensive stability analysis for the same airfoil flow at various angles of attack using a direct and adjoint operator approach [6] and a forced Navier-Stokes (N-S) equation approach [7–9]). Numerical results of both approaches favorably confirmed the existence of acoustic feedback mechanism and its physics was studied in some detail.

The control of undesirable airfoil tonal noise at low Reynolds number has gained significant attention and a number of passive and active methods have been proposed over the years. Examples of the prominent passive methods include the modification of airfoil geometry via a sawtooth shaped trailing edge [10], trailing edge serrations [11], perforated trailing edge [12], trailing edge brushes [13], and leading edge modifications [14]. In addition, a porous trailing edge is shown to reduce noise level at low frequencies but its high frequency components are amplified due to modified surface roughness [12]. Application of brushes is found to reduce the noise by a fair amount without any disadvantage at high frequencies [15]. Although porous trailing edge and brushes are effective in noise reduction, there are certain limitations in their implementation as the pores and brushes on these installations may collect dirt during operation and become ineffective quickly. Hansen et al. [14] applied serration treatment on the airfoil leading edge and claimed a significant reduction of the tonal noise. Unfortunately, there is a serious collateral effect with such modification as the aerodynamic performance of the airfoil was found to be seriously compromised. On the other hand, Wang [16]

successfully made use of blade trailing edge perforations to reduce tonal noise radiation from the contra-rotating fan models in his experiments but it also came at a cost of a penalty in the overall fan aerodynamic performance.

Wu et al. [17] recently proposed an alternate idea for airfoil tonal noise reduction that is radically different from those reported in the literature. Their approach aims to weaken, or even eliminate, the unsteady flow fluctuations induced inside airfoil boundary layer before they reach airfoil trailing edge and scatter as noise radiation. It essentially makes use of an elastic panel flush-mounted on airfoil surface which is excited by the oncoming flow fluctuations convected with the airfoil boundary layer flow. If the panel is so designed that it responds to vibrate with any of its natural frequencies, panel structural resonance may occur. Similar flow-structure interaction phenomenon was observed in a previous experimental and numerical study of aerodynamic and structural resonance of an elastic airfoil exposed to excitation by oncoming periodic discrete vortices, which were produced by two upstream cylindrical vortex generators [18]. Their results clearly illustrate that when the elastic airfoil is subjected to an oncoming excitation frequency that is close to any of its fluid-loaded natural frequencies, it will exhibit structural resonance and eventually run into limit cycle oscillation. In this situation the airfoil absorbs the kinetic energy carried by the oncoming vortical flow to sustain its flow-induced resonant vibration. The proposed approach aims to leverage a similar flow energy absorption phenomenon by using an elastic panel so as to greatly suppress the boundary layer flow unsteadiness before their eventual scattering as noise. The aeroacoustic feedback loop is weakened and the airfoil tonal noise is thus reduced. Essentially, there are two advantages with the proposed approach. Firstly, although the panel is set to vibrate in resonance, its vibration displacement should be small as compared to the airfoil chord, given the comparatively weak flow fluctuation amplitudes than those reported in Luk et al. [18]. This would lead to a weak distortion of streamlines locally around the elastic panel, which would result in a very weak modification of pressure distribution around the airfoil. Secondly, the panel acts to absorb flow fluctuation energy via a reactive mechanism rather than through a dissipative mechanism so the airfoil skin friction drag is effectively not influenced. As such, the proposed approach would be able to reduce the airfoil tonal noise without penalizing the airfoil aerodynamic performance. However, there is a potential drawback with their approach. Leung and So [19] carried out a detailed numerical study of flow-induced vibration of the vortex-airfoil system and their results showed that an elastic airfoil in aerodynamic or structural resonance may radiate loud loading noise. Similar phenomenon may occur with the proposed approach of Wu et al. [17]. There is a possibility that whilst the elastic panel in structural resonance is absorbing energy from boundary layer flow fluctuations, its own flow-induced vibration might radiate overwhelming loading noise with a level comparable to, or even higher than, that of original airfoil tonal noise, so that an overall noise amplification rather than reduction is achieved. This suggests the necessity of careful panel design in adopting the proposed ideas for airfoil tonal noise mitigation.

In principle, the feasibility of an elastic panel design for noise reduction can be explored in detail with high-fidelity direct aeroacoustic simulation (DAS) (e.g. Lam et al. [20]) or such sophisticated experimental techniques as in Arcondoulis et al. [21]. However, it is too prohibitive by virtue of the resources and time required to search for an

optimal design with these approaches, because of the vast design space of multiple panel physical parameters. It would be beneficial for developing the noise reduction idea if there is a design exploration methodology which allows much quicker panel design iterations with inputs of reasonable approximation of key noise production physics. Therefore, the present Note serves to report the development and progress of such quick design exploration methodology. Details of the methodology and its selected results are given in forthcoming sections.

II. Perturbation Evolution Method for Airfoil Flow

In brief the proposed methodology is entirely based on the analysis of evolution of introduced weak perturbation but it is initiated with information available from DAS solution of rigid airfoil. The required information includes the base flow obtained from time-averaging the DAS time-stationary solution and the flow characteristics of rigid airfoil. The former is taken as the base flow input for perturbation evolution method whereas the latter helps set the physical and material parameters for the design of elastic panel as well as its location. Numerical results show that a typical calculation with perturbation evolution method for an airfoil with elastic panel takes significantly shorter time required for its corresponding full DAS calculation. The time saving allows design iteration within the multiple panel parameters space for optimal noise reduction in a much quicker manner. Once determined, the optimal panel design can be incorporated into DAS calculation, or experimental study, for ascertaining the actual effectiveness of noise reduction.

In this section the perturbation evolution method adopted for the present study and its adaptation for analysis of airfoil flow with flow-induced panel vibration is described. The method is similar to stability analysis in its implementation as the techniques of classical linear stability analysis are widely used in boundary layer transition studies and provides an effective way to describe hydrodynamic stability responses over base shear flows qualitatively and quantitatively [22–24]. Although the classical linear stability analysis approach shows success in many studies of boundary layer transition and/or separation, its requirement of a quasi-parallel incompressible steady base flow makes its application to the present study of airfoil tonal noise generation problem largely impractical. Jones and his colleagues [8, 9] attempted to circumvent this limitation with an alternative numerical approach. Their approach embraces essentially the same sense of classical linear stability analysis but it is applicable for compressible flow problems with non-parallel base flow. They studied the flow stability characteristics of flow past a NACA 0012 airfoil at $M = 0.4$ and $AoA = 5^\circ$ by solving the compressible N-S equations directly with additional forcing terms. The forcing terms were carefully prescribed so that in absence of any introduced perturbation, the time steadiness of the initial condition (i.e. the base flow) can be guaranteed over a long time marching of the numerical solution. The stability analysis calculation was started after introducing a weak flow perturbation into the steady non-parallel compressible base flow and the subsequent flow perturbation responses and interactions are evolved with time marching of the forced equation. Their calculated flow stability characteristics were able to delineate clearly the role of separation bubble dynamics in airfoil tonal noise generation and subsequent acoustic feedback. It must be borne in mind that a proper choice of the base flow is of critical

importance to the successful application of the approach [9].

In the present study, we attempt a similar numerical approach to Jones et al. [8] for exploring the potential of utilizing flow-induced structural resonance of a flush-mounted elastic panel to manipulate boundary layer instability for reducing tonal noise. A brief of its adaptation to the present problem is given below. Choosing the airfoil chord, free-stream density and free-stream velocity as reference parameters, the normalized compressible N-S equations in two dimensions with a constant forcing term $\boldsymbol{S}$ may be written in strong conservative form as

$$\frac{\partial \boldsymbol{U}}{\partial t} + \frac{\partial \boldsymbol{F}}{\partial x} + \frac{\partial \boldsymbol{G}}{\partial y} = \boldsymbol{S} \tag{1}$$

where $\boldsymbol{U} = [\rho, \rho u, \rho v, \rho E]^T$, $\boldsymbol{F} = [\rho u, \rho u^2 + p - \tau_{xx}/Re_c, \rho uv - \tau_{xy}/Re_c, (\rho E + p)u - (\tau_{xx}u + \tau_{xy}v - q_x)/Re_c]^T$, $\boldsymbol{G} = [\rho v, \rho uv - \tau_{xy}/Re_c, \rho v^2 + p - \tau_{yy}/Re_c, (\rho E + p)v - (\tau_{xy}u + \tau_{yy}v - q_x)/Re_c]^T$ where $E, \tau_{xx}, \tau_{xy}, \tau_{yy}, q_x$ and q_y followed the description given in [25]. Given a base flow for Eq. 1, we introduce an infinitesimal perturbation to start the analysis calculation. We may write $\boldsymbol{U}(x, y, t) = \boldsymbol{U}_{base}(x, y) + \boldsymbol{U'}(x, y, t)$ and take the forcing term derived from spatial gradients of the base flow, so Eq. (1) becomes

$$\frac{\partial(\boldsymbol{U}_{base} + \boldsymbol{U'})}{\partial t} + \left(\frac{\partial \boldsymbol{F}}{\partial x} + \frac{\partial \boldsymbol{G}}{\partial y}\right)_{base} + \left(\frac{\partial \boldsymbol{F}}{\partial x} + \frac{\partial \boldsymbol{G}}{\partial y}\right)' = \boldsymbol{S} = \left(\frac{\partial \boldsymbol{F}}{\partial x} + \frac{\partial \boldsymbol{G}}{\partial y}\right)_{base}$$

$$\Rightarrow \frac{\partial\,(\boldsymbol{U}_{base} + \boldsymbol{U'})}{\partial t} + \left(\frac{\partial \boldsymbol{F}}{\partial x} + \frac{\partial \boldsymbol{G}}{\partial y}\right)' = 0$$

$$\Rightarrow \frac{\partial \boldsymbol{U'}}{\partial t} + \left(\frac{\partial \boldsymbol{F}}{\partial x} + \frac{\partial \boldsymbol{G}}{\partial y}\right)' = 0, \tag{2}$$

as the base flow is steady, i.e. $\partial \boldsymbol{U}_{base}/\partial t = 0$. Note that the homogeneous Eq. (2) has the same mathematical expression of the full nonlinear N-S equations for ordinary DAS calculation [26] but all the primitive variables are replaced by their perturbations in the flux variables $\boldsymbol{U}$, $\boldsymbol{F}$ and $\boldsymbol{G}$. Similar to DAS calculation, its solution should properly capture the nonlinear evolution and interactions of all flow perturbation, including acoustic disturbances, over a prescribed base flow. Therefore, we adopt the same numerical framework for solving Eq. (2) due to its proven capability of resolving correctly the coupling between the scale disparate unsteady aerodynamics and acoustics of complex airfoil [25]. This capability is particularly important in the perturbation evolution method employed in the present study. As seen in forthcoming discussions, it allows to capture the nonlinear interaction associated with airfoil aeroacoustic feedback loop even though the analysis is initiated with an imposed perturbation with amplitude orders of magnitude weaker. The DAS numerical framework is solved with the conservation element and solution element (CE/SE) scheme. Lam et al. [20, 26] systemically validated and consolidated the capability of CE/SE in capturing interactions between flow and acoustics accurately in a class of benchmark aeroacoustic problems at low Mach number.

The nonlinear dynamic response of the elastic panel is modeled by solving the one-dimensional plate equation to the simplest approximation [27]. The normalized governing equation for panel displacement can be written as

$$D_{EP}\frac{\partial^4 w}{\partial x^4} - (T_{EP} + N_{EP})\frac{\partial^2 w}{\partial x^2} + \rho_{EP} h_{EP}\frac{\partial^2 w}{\partial t^2} + C\frac{\partial w}{\partial t} + K_{EP} w = p_{ex} \tag{3}$$

where w is the panel displacement, $D_{EP} = \hat{D}_{EP}/\hat{\rho}_0 \hat{a}_0^2 \hat{c}^3$ is the panel bending stiffness, $T_{EP} = \hat{T}_{EP}/\hat{\rho}_0 \hat{a}_0^2 \hat{c}$ is the external tensile stress in tangential direction, $N_{EP} = (E_{EP} h_{EP}/2L_{EP}) \int_0^{L_{EP}} (\partial w/\partial x)^2 dx$ is the internal tensile stress in the tangential direction, $C = \hat{C}/\hat{\rho}_0 \hat{a}_0$ is the structural damping coefficient of panel, $K_{EP} = \hat{K}_{EP}\hat{c}/\hat{\rho}_0 \hat{a}_0$ is the stiffness of the foundation supporting the panel and $p_{ex} = \hat{p}_{ex}/\hat{\rho}_0 \hat{a}_0^2$ is the net pressure exerted on the panel surface. In the present study, we have considered a very thin elastic panel which is similar to membrane, therefore, structural damping C_{EP}, panel internal tension N_{EP} and bending stiffness D_{EP} are taken as zero [28]. The panel dynamic equation (Eq. (3)) is solved by the standard finite difference method. The nonlinear coupling between flow fluctuation and panel structural dynamics is resolved with a monolithic scheme developed by Fan et al. [28]. In essence, the scheme treats the fluid/panel system as a single entity and includes the effects panel dynamics in an extra source term (not the $\boldsymbol{S}$ in Eq. (1)) in the CE/SE numerical model which is then solved with a Newton iteration method. It is fully validated with a series of benchmark aeroacoustic-structural interaction problems and is proven to accurately resolve aeroacoustic-structural coupling of various complexity over a long solution time marching. No-slip boundary conditions are applied to all airfoil and panel surfaces. The same convergent mesh and time step size given in Wu et al. [17] are used in the present study.

III. Results and Discussions

We aim at exploring the potential of utilizing elastic panel to reduce the tonal noise of a NACA 0012 airfoil at AoA = 5° with freestream at M_a = 0.4 and $Re_c = 5 \times 10^4$ using the perturbation evolution method described in Section II. In the absence of any introduced perturbation $\boldsymbol{U}_{base}$ has to remain unchanged when it is marched with Eq. (1) over a long time; otherwise, the solution will be driven by the evolution of base flow itself, rather than by the intended evolution of flow instability characteristics, to rapid solution divergence. Jones et. al [8] attempted different ways of producing base flow solutions for their stability analysis. They found that the time average of flow solution produced by direct simulation of the original problem is a promising choice. We adopt the same approach to produce the base flow for the present study. Wu et al. [17] carried out a full DAS calculation of tonal noise generation by the same rigid airfoil with same flow conditions. The unsteady solution was fully validated and shown able to accurately reproduce all the key tonal noise generation features reported in previous numerical studies by means of compact finite difference calculation [7, 8]. We have taken ten cycles of the DAS time stationary solution and averaged them in time to produce the base flow solution $\boldsymbol{U}_{base}$ (Fig. 1(a) and (b)). The quality of $\boldsymbol{U}_{base}$ is checked by solving it as initial condition with Eq.(2) in the absence of any flow perturbation. The deviation of flow solution from initial $\boldsymbol{U}_{base}$ during time marching is

shown in Fig. 1(c). Very little deviation prevails in the beginning of the calculation which promptly becomes saturated with a numerical error level well below 10^{-10}. This error level is five orders of magnitude weaker than the introduced excitation amplitude and, as shown clearly in subsequent discussions, is around six orders of magnitude weaker than the perturbation evolution method solution. Therefore, the $\boldsymbol{U}_{base}$ adopted is considered to satisfy the requirement $\partial \boldsymbol{U}_{base}/\partial t = 0$ effectively.

The prescription of weak perturbation for initiating the evolution of flow instability requires careful consideration in the present study. Jones et al. [8] applied periodic volume forcing within the airfoil boundary layer. Alternatively Fosas de Pando et al. [6] made use of an artificial weak divergence-free Gaussian pulse released at an upstream location very close to the airfoil as the external excitation. They allowed the artificial pulse to convect freely with the evolution of numerical solution to hit the airfoil leading edge and produce the actual flow perturbations required for subsequent analysis. We initially adopted a similar way by introducing a weak Gaussian pulse near airfoil leading edge for perturbation evolution analysis. Whilst the pulse is able to induce the occurrence of the aeroacoustic feedback loop as reported in previous studies, it is only able to induce the panel to give a vibration pulse in every cycle of feedback rather than sustaining a continuous vibration to its resonance throughout the entire feedback loop process. Hence, excitation by a pulse could not be utilized in the present study. We changed to utilize broadband acoustic excitation in our study which can effectively produce weak perturbations within the flow continuously. Such excitation also mimics the continuous excitation experienced in actual flow past airfoil. With the introduction of broadband acoustic excitation, the hydrodynamic instabilities could be generated within the airfoil boundary layer [8]. The broadband acoustic excitation function is defined as,

$$p'_{inc} = p_A \sum_{n=1}^{100} \sin(2\pi t f_{exc,n} + \phi_n), \tag{4}$$

where p_A is pressure amplitude which is constant to wide range of frequencies $f_{exc,n}$ ranging from 0.1 to 10 with a uniform spacing of $\Delta f_{exc,n} = 0.1$, and uniformly random phase ϕ_n. A weak excitation of $p_A = 10^{-5}$ is introduced near the leading edge of airfoil at a location $(x, y) = (-0.015, -0.01)$ to generate weak artificial perturbations. When the acoustic excitation interacts with leading edge of airfoil, a downstream travelling wavepacket over the airfoil suction surface is generated. As a result of broadband nature of excitation, it would excite a number of panel natural modal frequencies. However, at the dominant frequency of naturally evolving boundary layer disturbance on airfoil suction surface the flow-induced structural resonance would occur and the panel would respond effectively in suppressing the flow instabilities in this condition. The numerical results show that the selected artificial disturbance is able to maintain its localized flow perturbation properties well during solution time marching.

A. Design of Elastic Panel

The primary goal of the present study is to explore the feasibility of suppression of airfoil tonal noise generation by the flow-induced vibration of an elastic panel mounted beneath airfoil boundary layer. Three major design parameters of the panel are important in achieving this purpose, namely its length, mounting location, and structural properties. We considered three panel designs in this study.

The panel is expected to be excited by the instability of growing boundary layer convecting over it in such a way that the flow perturbation energy is effectively converted to sustain panel vibration. As such the panel must be set at a location where its flow-induced vibration is easy to occur. Its choice is aided by the knowledge of flow characteristics of the natural boundary layer of the original airfoil flow which can be easily derived from the time-stationary DAS solution of Wu et al. [17]. In essence, we capture the time traces of flow fluctuation at every location along a contour well close parallel to airfoil suction surface. We then put every time trace through FFT to obtain its spectrum from which the characteristic frequencies and amplitudes of flow fluctuation are identified and determined. The details of the calculation is referred to Wu et al. [17]. The FFT results reveal that the natural airfoil boundary layer growth are dominated by two frequencies, namely the fundamental $(f_{bl})_0 = 3.37$ and the first harmonic $(f_{bl})_1 = 6.67$. The distribution of the amplitudes of velocity fluctuation v' at $(f_{bl})_0$ and $(f_{bl})_1$ along airfoil chord is shown in Fig. 2. Both amplitudes start to increase at $x \geq 0.27$ and grow within $0.4 \leq x \leq 0.45$. The amplitude of $(f_{bl})_0$ grows remarkably to reach its plateau of 0.0425 at $x \sim 0.5$, stays there up till $x \sim 0.57$, then drops rapidly to a dip at $x \sim 0.65$, and eventually grow mildly again. The amplitude of $(f_{bl})_1$ appears to grow in a more gradual fashion and fluctuates mildly around a value of 0.0125 beyond $x \sim 0.57$. It is interesting to see that the region for drastic stability amplification, i.e. $0.27 \leq x \leq 0.57$, is coincident with the emergence of separation bubble on airfoil suction surface. Such observation is consistent with the instability wave analysis by solving Orr-Sommerfeld equation [7]. The location of panel is set with careful consideration of the flow characteristics in Fig. 2. The works of Luk et al. [18] and Leung & So [19] show that maximum vibration response of an elastic airfoil can be achieved when its chord length is comparable to the wavelength of oncoming flow excitation. Thus, in the same spirit of these two works, the first panel is set with length $L_{EP} = 0.05$ comparable to the length of $(f_{bl})_0$ amplitude plateau and thickness $h_{EP} = 0.009$. It is placed with panel leading edge at $x_{EP} = 0.45$ so as to allow energy transfer from fully established flow instability to vibrating panel. This panel design is labeled as $EP2$. Another panel, labeled as $EP1$, of same length is set at $x_{EP} = 0.40$ to study the feasibility of diverting the energy transfer to panel vibration from sustaining the rapid stability growth at $x \sim 0.5$. Finally a third panel, labeled as $EP3$, is set close to airfoil trailing edge at $x_{EP} = 0.90$ so as to study the feasibility of reducing flow fluctuation energy that will scatter to noise at airfoil trailing edge. Furthermore, one has to note if the mounting of each initially flat panel distorts the airfoil profile locally. The offset δ_{EP} of each panel from local radii of curvature $r(x) = \sqrt[3]{\left(1 + (dy/dx)^2\right)} / \left|d^2y/dx^2\right|$ where $y = y(x)$ is the NACA 0012 profile, at panel center is evaluated and listed in Table 1. It can be seen that the panel offset is in fact extremely small as compared to airfoil chord so that

Table 1 Listing of normalized elastic panel parameters. Stainless steel is assumed for material properties.

	Case	Geometrical parameters				Material properties		Panel natural frequency		
		x_{EP}	δ_{EP}	L_{EP}	h_{EP}	T_{EP}	ρ_{EP}	$(f_{EP})_1$	$(f_{EP})_2$	$(f_{EP})_3$
Non-resonant panel	$EP1_{NR}$	0.40	9.2 x 10^{-5}	0.05	0.009	4.023	6367.35	2.6453 (79%)	5.2909 (157%)	7.9366 (236%)
	$EP2_{NR}$	0.45	7.96 x 10^{-5}							
	$EP3_{NR}$	0.90	4.51 x 10^{-5}							
Resonant panel	$EP1_R$	0.40	9.2 x 10^{-5}	0.05	0.009	0.725	6367.35	1.123 (33%)	2.246 (67%)	3.369 (100%)
	$EP2_R$	0.45	7.96 x 10^{-5}							
	$EP3_R$	0.90	4.51 x 10^{-5}							

the streamlines of base flow in proximity of panels can be considered effectively unaltered. A schematic sketch of the flow problem and locations of elastic panels are shown in Fig. 3.

Two types of panel structural properties are set. One type is set to make its natural modal frequencies almost the same as the dominant $f_{bl,0}$ so that flow-induced panel resonance is easy to occur. The normalized frequency of the n^{th} panel vibration mode taking the effect of fluid loading into account can be estimated as [29],

$$(f_{EP})_n = \frac{n}{L_{EP}}\sqrt{\frac{T}{\rho_{EP}h_{EP}}}\Bigg/\sqrt{1+\frac{L_{EP}}{\pi n \rho_{EP}h_{EP}}} \tag{5}$$

Given the values of L_{EP} and h_{EP} set, the closest panel natural frequency possible is f_{EP1} = 3.37. The second type of panel is set with its natural modal frequencies distant from any f_{bl} so that panel resonance is avoided. The details of all panel parameters set for the present study are given in Table 1.

B. Verification of Proposed Methodology

The effect of elastic panel in each EP case is explored from a comparison of its numerical results with those obtained from its reference calculation with the panel replaced by the original rigid airfoil profile. The latter is labeled as RS. Before starting the comparison it is important to check if the perturbation evolution analysis for RS case is able to reproduce the key physical processes responsible for tonal noise generation. The evolution of flow instability is analyzed in terms of the instantaneous snapshots of distribution of velocity fluctuation v' (Fig. 4). The introduced excitation perturbation is convected following a streamline of base flow and initiates a wavepacket triggered by the

local inflectional velocity profiles of the base flow. The wavepacket is found to possess similar characteristics of Tollmien-Schlichting (T-S) waves as observed in laminar boundary layers over a flat plate [30]. While the wavepacket is convecting downstream, its amplitude continues to grow with a mechanism related to Kelvin-Helmholtz (K-H) instabilities within the shear layer inside separation bubble region (cf. Fig. 2) and attains its maximum at the moment it reaches the reattachment point (Fig. 4a). The amplitude of the wavepacket then weakens due to a sudden change in stability characteristics between separation bubble and reattached flow. The wavepacket grows strong again in a similar fashion to K-H instabilities inside reattached flow region until it hits the airfoil trailing edge where the wavepacket scatters to acoustic wave radiating away from surface and pressure sides of the airfoil. It is interesting to note that the wavelengths of the scattered wave and secondary instability are longer than the K-H ones. The K-H instabilities also gives wake (Fig. 4b). The acoustic wave propagates upstream, hits the separation point again and produces a second wavepacket (Fig. 4c). It is important to realize that this wavepacket is triggered by the receptivity of boundary layer to free-stream disturbances originated downstream. The flow instabilities and acoustic wave appear continuously with the repetition of aeroacoustic feedback loops (Fig. 4d). These observations are consistent with those reported in previous studies calculated with different numerical approaches [6, 8]. The consistency clearly indicates that the present perturbation evolution method with broadband excitation is able to capture the aeroacoustic feedback loop responsible for airfoil tonal noise generation correctly and provide a quality reference solution for illustrating the effects of elastic panel. In fact same aeroacoustic feedback loops are also observed in the full DAS calculation of the same airfoil flow [17].

Now an elastic panel is readily installed onto airfoil suction surface for studying its potential for airfoil tonal noise reduction. However, in view of the rationale of proposed design methodology, a base flow with elastic panel installed is generally not known *a priori* as its DAS calculation has not yet been carried out. To circumvent this difficulty it is proposed to adopt the base flow of RS case in perturbation evolution method calculations of EP cases. This choice is based on two assumptions. The first arises from the benefit of the chosen short panel length as discussed in Section A. The second arises from the fact that the setting of perturbation evolution method allows the elastic panel to be primarily responsive only to the convecting flow instability and scattered acoustic disturbances whose velocity fluctuation magnitudes are at least two orders of magnitude weaker than the steady base flow. The panel vibration response is expected to follow the same order of magnitude so it should not modify the base flow significantly. It is essential to verify these assumptions before proceeding to an extensive study of noise reduction with various elastic panel designs. For this purpose, an additional DAS calculation is carried out with an arbitrary choice of panel design, say $EP1_{NR}$. Its base flow solution is obtained from averaging the time stationary solution in time for comparison with RS base flow. Fig. 5(a) shows the distribution of percentage deviation (i.e. $|(EP1_{NR})_{base}$ - $(RS)_{base}|$ / $|(RS)_{base}|$) between the total velocity fields of two base flow solutions. It shows that there is modification in the proximity of elastic panel but its deviation is almost two orders of magnitude weaker than the velocity fluctuations obtained from the

Table 2 A comparison of level of noise reduction of $EP1_{NR}$ case from perturbation evolution method and DAS solutions.

	Perturbation evolution method	DAS
Average $\Delta SPL_{reduction}$	1.20 dB	1.1 dB
Maximum $\Delta SPL_{reduction}$ / θ_{max}	1.50 dB / 130°	1.45 dB / 120°

results by perturbation evolution method. No significant difference between mean flows of RS and $EP1_{NR}$ cases is observed. Furthermore, the azimuthal distributions of acoustic p'_{rms} captured at a radius of three chord lengths from trailing edge obtained from perturbation evolution method and DAS solutions are compared in Fig. 5(b) which shows a good qualitative agreement. The levels of noise reduction $\Delta SPL_{reduction} = 20 \times log_{10}\left(p'_{rms,EP}/p'_{rms,RS}\right)$ derived from two types of calculations are found in excellent agreement too (Table 2). Therefore, all these evidence lend strong concrete support to the adoption of RS base flow as a reasonably good approximation for base flow for perturbation evolution method calculation of EP cases. The affirmative results also reflect that the proposed methodology is able to correctly predict the trend of noise reduction by the elastic panel in actual flow by virtue of its capability of capturing the fundamental airfoil tonal noise generation processes as indicated in early discussions. It is worthy noting that for the perturbation evolution method a simulation requires a time marching within 10 non-dimensional time units with a time step size of 10^{-5} to reach saturated regime. However a typical DAS calculation has to march in time over 120-150 non-dimensional time units to reach time stationarity. Hence, a significant saving of more than 90% of actual calculation time is achieved using the perturbation evolution method.

C. Noise Reduction by Elastic Panels

The focus of forthcoming discussion is put in the region around the airfoil trailing edge where the oncoming flow instability scatters into airfoil tonal noise. Fig. 6 (first row) shows a comparison of transverse velocity fluctuation v' of flow instability captured at x = 0.99c from the solutions of non-resonant $EP1_{NR}$ and resonant $EP1_R$ cases during t = 4-8 where the feedback loop has been established already. Regular wavepackets due to external excitation and feedback loop can be observed clearly. The flow-induced vibration of elastic panel appears to provide continuous suppression of flow instability growth. The extent of instability suppression appears strongly dependent on panel structural properties. It is stronger in case $EP1_R$ than that in case $EP1_{NR}$. This observation provides good support to the envisage that a resonant panel absorbs the flow energy more effectively and leaves less flow distortion for the scattering at airfoil trailing edge. To further illustrate this view we define a consistent time window of a single wavepacket in each case and calculate the v'_{rms} values within this time window of the particular wavepacket. The calculated v'_{rms} values are listed in Table 3. The percentage loss of energy from the respective RS case is also given together in the brackets. It is evident that the reduction of flow energy is fairly uniform with a non-resonant panel but it appears to differ in intensity when a

Table 3 Effect of the presence of elastic panel on v'_{rms} in $EP1$, $EP2$ and $EP3$ cases.

Location	RS	$EP1_{NR}$	$EP1_R$	$EP2_{NR}$	$EP2_R$	$EP3_{NR}$	$EP3_R$
$x = 0.8$	2.0096 x 10^{-3}	1.6482 x 10^{-3} (-17.98%)	1.5077 x 10^{-3} (-24.97%)	1.8330 x 10^{-3} (-8.78%)	1.7987 x 10^{-3} (-10.49%)	2.0017 x 10^{-3} (-0.39%)	1.9705 x 10^{-3} (-1.94%)
$x = 0.9$	2.3637 x 10^{-3}	1.9091 x 10^{-3} (-19.23%)	1.6910 x 10^{-3} (-28.46%)	2.1919 x 10^{-3} (-10.23%)}	2.0173 x 10^{-3} (-14.65%)	2.3259 x 10^{-3} (-1.60%)	2.3160 x 10^{-3} (-2.02%)
$x = 0.99$	4.6241 x 10^{-3}	3.4304 x 10^{-3} (-25.81%)	2.9992 x 10^{-3} (-35.13%)	3.9466 x 10^{-3} (-14.65%)	3.7207 x 10^{-3} (-19.53%)	4.4486 x 10^{-3} (-3.79%)	4.4466 x 10^{-3} (-3.83%)

resonant panel is mounted. The suppressed flow instability should produce less effective scattering at trailing edge and subsequently lower noise radiation. This inference receives concrete support from the acoustic solutions shown in Figs. 7(a) and 7(b). The acoustic solution within the sector $|\theta| \leq 30°$ is ignored because the chaotic solution right downstream airfoil trailing edge makes the determination of acoustics there inaccurate. These figures show that the noise radiation pattern looks like a dipole skewed towards upstream with stronger radiation from airfoil suction surface than from pressure surface. The strongest radiation goes along $\theta \sim 130°$ and $220°$ respectively. More noise reduction toward upstream is observed than downstream. A resonant panel achieves an average $\Delta SPL_{reduction} \sim 2.1$ dB around most θ values with maximum reduction of ~ 2.4 dB along $\theta \sim 130°$. However, a non-resonant panel achieves an average of ~ 1.2 dB reduction and its maximum of ~ 1.5 dB only.

The transverse velocity fluctuations v' of flow instability for $EP2$ cases are shown in Fig. 6 (second row). Generally similar effects of elastic panel to $EP1$ cases can still be observed but the suppression of flow instability is less pronounced even though the elastic panel location coincides with the occurrence of strongest natural boundary layer instability Fig. 2. All the flow instability evolution patterns are very similar to $EP1$ cases (Fig. 6). The v'_{rms} values are evaluated in the same way as for $EP1$ cases and the results are shown in Table 3. They show transfer of flow energy to vibrating panel but their effectiveness are reduced by half for both non-resonant and resonant panels. The directivity of noise radiation is similar to $EP1$ cases (Fig. 7(c)). Fortunately, there is still noise reduction as observed in Fig. 7(d). A non-resonant panel achieves a fairly uniform noise reduction with an average $\Delta SPL_{reduction} \sim 0.45$ dB around the airfoil with maximum reduction of ~ 0.6 dB but a resonant panel enhances the noise reduction to $\Delta SPL_{reduction} \sim 0.7$ dB with maximum reduction of ~ 0.84 dB.

Fig. 6 (third row) shows the transverse velocity fluctuations v' of flow instability for $EP3$ cases. In contrast with $EP1$ and $EP2$ cases, the $EP3$ panel is at a distance of only 0.05c from airfoil trailing edge and the sudden change of pressure behind the airfoil imposes an irregular growth on the flow instability. The calculated v'_{rms} values for both resonant and non-resonant cases are shown in Table 3. The directivity of noise radiation and noise reduction are shown

in Fig. 7(e) and (f). This time the noise radiation gives a different pattern from $EP1$ and $EP2$ cases where the reduction as well as amplification in pressure fluctuations can be observed. Both resonant and non-resonant panels provide more or less the same noise reduction pattern with strongest reduction of around 0.5 dB at $\theta \sim 170°$. However, regions around $\theta \sim$ 50-60°, $\theta \sim$ 120-150° and $\theta \sim$ 180-240° shows some noise amplification as well. Hence, it implies that the location of panel near the trailing edge of airfoil is not effective in suppressing flow instabilities and can result in noise amplification as well.

D. Structural Response of Elastic Panel

The response of elastic panel due to boundary layer instabilities and subsequent fluid-structure interactions for $EP1$, $EP2$ and $EP3$ are shown in Fig.8. A snapshot at t = 6 is chosen as a reference for all panel configurations based on the moderate fluctuations at this instance observed in v'_{rms} plots. The parameters for resonant panel are set in a manner that flow-induced structural resonance occurs at the third natural mode as already shown in Table 1.

It is evident in Fig.8(a) that $EP1_R$ vibrates at its third natural mode with stronger amplitude as compared to first mode for $EP1_{NR}$. The fact that $EP1_R$ vibrates in the desired third natural mode validates our panel design methodology to achieve structural resonance in the presence of fluid loading on the panel. Since $EP1_R$ tension is much lower than $EP1_{NR}$ whose frequency is closest to $(f_{bl})_0$. It implies that resonant panel is much more compliant to flow-induced loading than non-resonant panel. Hence, it is able to effectively absorb more energy from the oncoming flow to sustain its resonance condition. The resulting phenomenon helps in weakening of T-S waves instabilities within the laminar boundary layer which ultimately helps in the reduction of noise level due to trailing edge scattering. Similar features can be observed for $EP2$ in Fig.8(b). Although $EP2_R$ vibrates at its third mode as designed, the noise suppression is much weaker than $EP1_R$. Though the resonant panel is able to allow transfer of energy from the incoming flow but its effectiveness is relatively reduced as boundary layer instability is the strongest at this panel location which is already indicated in Fig. 2. Hence, it poses an opportunity for further investigation in design of panel with better characteristics without inducing other undesired instabilities such as flutter or divergence. Fig.8(c) shows a similar pattern for both $EP3_R$ and $EP3_{NR}$, but there exists a non-uniformity in panel response in terms of amplitude and mode shape for both resonant and non-resonant panels. This non-uniform vibrational response possibly explains the reason for low noise level reduction and even amplification for both resonant and non-resonant panel configurations at different azimuth locations as observed in Fig. 7(f).

Time history of panel velocity for elastic panels at center location of each panel is plotted and shown in Fig. 8 (right column). A span of 6-10 time units is chosen for brevity as the panel has sustained sufficient vibrational velocity during this period. It can be observed that $EP1_R$, $EP2_R$ and $EP3_R$ have much higher vibrational velocities than their non-resonant counterparts. Furthermore, the magnitude of velocity for $EP1_R$ is much higher than $EP2_R$ and $EP3_R$. Hence, it is able to absorb much higher energy from the hydrodynamic instabilities to sustain its vibration than $EP2_R$

and $EP3_R$. Also, the vibrational behavior of all resonant panels is observed to be much more uniform and periodic than non-resonant panels. Hence, the resonant panels can sustain the dynamical behavior in their designed mode. Therefore, it can be easily ascertained that the resonant panels are much better choice for tonal noise reduction for present study.

E. Conclusions

This Note reports an exploratory study of the feasibility of airfoil tonal reduction by means of an elastic panel flush-mounted on airfoil suction surface. The airfoil takes a NACA 0012 profile at an angle of attack of 5° with chord-based Reynolds number of 5×10^4 and Mach number of 0.4. The panel is expected to absorb the energy of boundary layer instabilities convecting with airfoil flow by means of its own flow-induced vibration. As such the flow fluctuation responsible for scattering at airfoil trailing edge as noise and the subsequent aeroacoustic feedback loop that underlies the sustained tonal noise radiation are weakened. A perturbation evolution method is adopted for the feasibility study of panel design due to its lower computational resource requirement than full direct aeroacoustic simulation. The base flow for the perturbation evolution method is obtained from averaging the time stationary solutions of accompanying direct aeroacoustic simulation (DAS) of same flow with fully rigid airfoil. In order to allow the elastic panel to set into continuous flow-induced vibration, the analysis is implemented with a broadband excitation instead of a discrete Gaussian pulse. The nonlinear equation is solved by the conservation-element and solution-element (CE/SE) method, whereas the panel dynamic equation is solved by the standard finite difference method. A monolithic coupling scheme is invoked for its capability of accurately resolving the nonlinear interaction between boundary layer instability and flow-induced panel vibration. The perturbation evolution method is applied with various panel structural parameters and panel locations and the resulting potential for reducing airfoil tonal noise is studied. Generally, all elastic panel designs yield varying levels of tonal noise reduction but maintain more or less the same directivity as the rigid airfoil. It implies that the existence of an elastic panel does not alter the nature of the aeroacoustic feedback loop but only modifies its effectiveness at reducing noise. It is found that a panel located just ahead of the sharp growth of natural boundary layer instability within the airfoil separation bubble provides the strongest reduction of instabilities that are responsible for scattering into noise at the airfoil trailing edge and, hence, provides the most noise reduction among all cases studied. A panel located at the plateau in the boundary layer instability amplitude or in the proximity of the airfoil trailing edge gives a much lower noise reduction. In addition, for a given panel location, higher noise reduction is achieved when the structural parameters of the panel are tuned in such a way that its fluid-loaded natural frequency is coincident with the dominant frequency of the flow fluctuation passing over it. A resonant panel in the best location is able to yield almost uniform azimuthal noise reduction of around 2.1 dB, whereas a non-resonant panel at the worst location gives only 0.5 dB noise reduction. Based on the results of the study, installation of a flush-mounted elastic panel is proven to be a feasible method for airfoil tonal noise reduction. Furthermore, the adopted perturbation evolution method appears to be a viable tool supporting quick panel design iterations to search for optimal noise reduction as it takes only around 10%

computational time of the corresponding DAS calculation. The time saving can then be spent on DAS calculation for the optimal panel design for gaining better understanding of the relevant physics of noise reduction.

Acknowledgments

The first and second authors gratefully acknowledge the research studentship tenable at Department of Mechanical Engineering, The Hong Kong Polytechnic University. The third and fourth authors gratefully acknowledge the support from the Research Grants Council of the Government of Hong Kong Special Administrative Region under Grant No A-PolyU503/15, and a research donation from the Philip K. H. Wong Foundation under grant number 5-ZH1X. The provision of computer times by University Research Facility in Big Data Analytics (UBDA) at The Hong Kong Polytechnic University is gratefully acknowledged.

References

[1] Brooks, T. F., Pope, D. S., and Marcolini, M. A., "Airfoil self-noise and prediction," *NASA Technical Report*, 1989, pp. 2–4.

[2] Paterson, R. W., Vogt, P. G., Fink, M. R., and Munch, C. L., "Vortex noise of isolated airfoils," *Journal of Aircraft*, Vol. 10, No. 5, 1973, pp. 296–302. https://doi.org/10.2514/3.60229.

[3] Tam, C. K. W., "Discrete tones of isolated airfoils," *The Journal of the Acoustical Society of America*, Vol. 55, No. 6, 1974, pp. 1173–1177. https://doi.org/10.1121/1.1914682.

[4] Arbey, H., and Bataille, J., "Noise generated by airfoil profiles placed in a uniform laminar flow," *Journal of Fluid Mechanics*, Vol. 134, 1983, pp. 33–47. https://doi.org/10.1017/S0022112083003201.

[5] Desquesnes, G., Terracol, M., and Sagaut, P., "Numerical investigation of the tone noise mechanism over laminar airfoils," *Journal of Fluid Mechanics*, Vol. 591, 2007, pp. 155–182. https://doi.org/10.1017/S0022112007007896.

[6] Fosas de Pando, M., Schmid, P. J., and Sipp, D., "A global analysis of tonal noise in flows around aerofoils," *Journal of Fluid Mechanics*, Vol. 754, 2014, pp. 5–38. https://doi.org/10.1017/jfm.2014.356.

[7] Jones, L. E., Sandberg, R. D., and Sandham, N. D., "Direct numerical simulations of forced and unforced separation bubbles on an airfoil at incidence," *Journal of Fluid Mechanics*, Vol. 602, 2008, pp. 175–207. https://doi.org/10.1017/S0022112008000864.

[8] Jones, L. E., Sandberg, R. D., and Sandham, N. D., "Stability and receptivity characteristics of a laminar separation bubble on an aerofoil," *Journal of Fluid Mechanics*, Vol. 648, 2010, pp. 257–296. https://doi.org/10.1017/S0022112009993089.

[9] Jones, L. E., and Sandberg, R. D., "Numerical analysis of tonal airfoil self-noise and acoustic feedback-loops," *Journal of Sound and Vibration*, Vol. 330, No. 25, 2011, pp. 6137–6152. https://doi.org/10.1016/j.jsv.2011.07.009.

[10] Avallone, F., Van Der Velden, W., Ragni, D., and Casalino, D., "Noise reduction mechanisms of sawtooth and combed-sawtooth trailing-edge serrations," *Journal of Fluid Mechanics*, Vol. 848, 2018, pp. 560–591. https://doi.org/10.1017/jfm.2018.377.

[11] Gruber, M., Joseph, P., and Chong, T. P., "Experimental investigation of airfoil self noise and turbulent wake reduction by the use of trailing edge serrations," *16th AIAA/CEAS aeroacoustics conference*, 2010, p. 3803. https://doi.org/10.2514/6.2010-3803.

[12] Geyer, T., Sarradj, E., and Fritzsche, C., "Measurement of the noise generation at the trailing edge of porous airfoils," *Experiments in Fluids*, Vol. 48, No. 2, 2010, pp. 291–308. https://doi.org/10.1007/s00348-009-0739-x.

[13] Finez, A., Jacob, M., Jondeau, E., and Roger, M., "Broadband noise reduction with trailing edge brushes," *16th AIAA/CEAS aeroacoustics conference*, 2010, p. 3980. https://doi.org/10.2514/6.2010-3980.

[14] Hansen, K., Doolan, C., and Kelso, R., "Reduction of flow induced airfoil tonal noise using leading edge sinusoidal modifications," *Acoustics Australia*, Vol. 40, No. 3, 2012, pp. 1–6.

[15] Herr, M., and Dobrzynski, W., "Experimental Investigations in Low-Noise Trailing Edge Design," *AIAA Journal*, Vol. 43, No. 6, 2005, pp. 1167–1175. https://doi.org/10.2514/1.11101.

[16] Wang, C., "Trailing Edge Perforation for Interaction Tonal Noise Reduction of a Contra-Rotating Fan," *Journal of Vibration and Acoustics*, Vol. 140, No. 2, 2018. https://doi.org/10.1115/1.4038253.

[17] Wu, D., Lam, G. C. Y., and Leung, R. C. K., "An Attempt to Reduce Airfoil Tonal Noise Using Fluid-Structure Interaction," *2018 AIAA/CEAS Aeroacoustics Conference*, 2018, p. 3790. https://doi.org/10.2514/6.2018-3790.

[18] Luk, K. F., So, R. M. C., Leung, R. C. K., Lau, Y. L., and Kot, S. C., "Aerodynamic and structural resonance of an elastic airfoil due to oncoming vortices," *AIAA Journal*, Vol. 42, No. 5, 2004, pp. 899–907. https://doi.org/10.2514/1.2246.

[19] Leung, R. C. K., and So, R. M. C., "Noise generation of blade–vortex resonance," *Journal of sound and vibration*, Vol. 245, No. 2, 2001, pp. 217–237. https://doi.org/10.1006/jsvi.2001.3575.

[20] Lam, G. C. Y., Leung, R. C. K., Seid, K. H., and Tang, S. K., "Validation of CE/SE scheme in low mach number direct aeroacoustic simulation," *International Journal of Nonlinear Sciences and Numerical Simulation*, Vol. 15, No. 2, 2014, pp. 157–169. https://doi.org/10.1515/ijnsns-2012-0118.

[21] Arcondoulis, E., Doolan, C. J., Zander, A. C., Brooks, L. A., and Liu, Y., "An investigation of airfoil dual acoustic feedback mechanisms at low-to-moderate Reynolds number," *Journal of Sound and Vibration*, Vol. 460, 2019, p. 114887. https://doi.org/10.1016/j.jsv.2019.114887.

[22] Mack, L. M., "Linear stability theory and the problem of supersonic boundary-layer transition," *AIAA Journal*, Vol. 13, No. 3, 1975, pp. 278–289. https://doi.org/10.2514/3.49693.

[23] Huerre, P., and Monkewitz, P. A., "Local and global instabilities in spatially developing flows," *Annual review of fluid mechanics*, Vol. 22, No. 1, 1990, pp. 473–537. https://doi.org/10.1146/annurev.fl.22.010190.002353.

[24] Reed, H. L., Saric, W. S., and Arnal, D., "Linear stability theory applied to boundary layers," *Annual review of fluid mechanics*, Vol. 28, No. 1, 1996, pp. 389–428. https://doi.org/10.1146/annurev.fl.28.010196.002133.

[25] Lam, G. C. Y., and Leung, R. C. K., "Aeroacoustics of NACA 0018 Airfoil with a Cavity," *AIAA Journal*, Vol. 56, No. 12, 2018, pp. 4775–4786. https://doi.org/doi.org/10.2514/1.J056389.

[26] Lam, G. C. Y., Leung, R. C. K., and Tang, S. K., "Aeroacoustics of duct junction flows merging at different angles," *Journal of Sound and Vibration*, Vol. 333, No. 18, 2014, pp. 4187–4202. https://doi.org/10.1016/j.jsv.2014.04.045.

[27] Dowell, E. H., *Aeroelasticity of plates and shells*, Vol. 1, Springer Science & Business Media, 1974.

[28] Fan, H. K. H., Leung, R. C. K., Lam, G. C. Y., Aurégan, Y., and Dai, X., "Numerical Coupling Strategy for Resolving In-Duct Elastic Panel Aeroacoustic/Structural Interaction," *AIAA Journal*, Vol. 56, No. 12, 2018, pp. 5033–5040. https://doi.org/10.2514/1.J057324.

[29] Blevins, R. D., *Formulas for natural frequency and mode shape*, RE Krieger, 1979.

[30] Ruban, A. I., "On the generation of Tollmien-Schlichting waves by sound," *Fluid Dynamics*, Vol. 19, No. 5, 1984, pp. 709–717. https://doi.org/10.1007/978-3-642-82462-3_39.

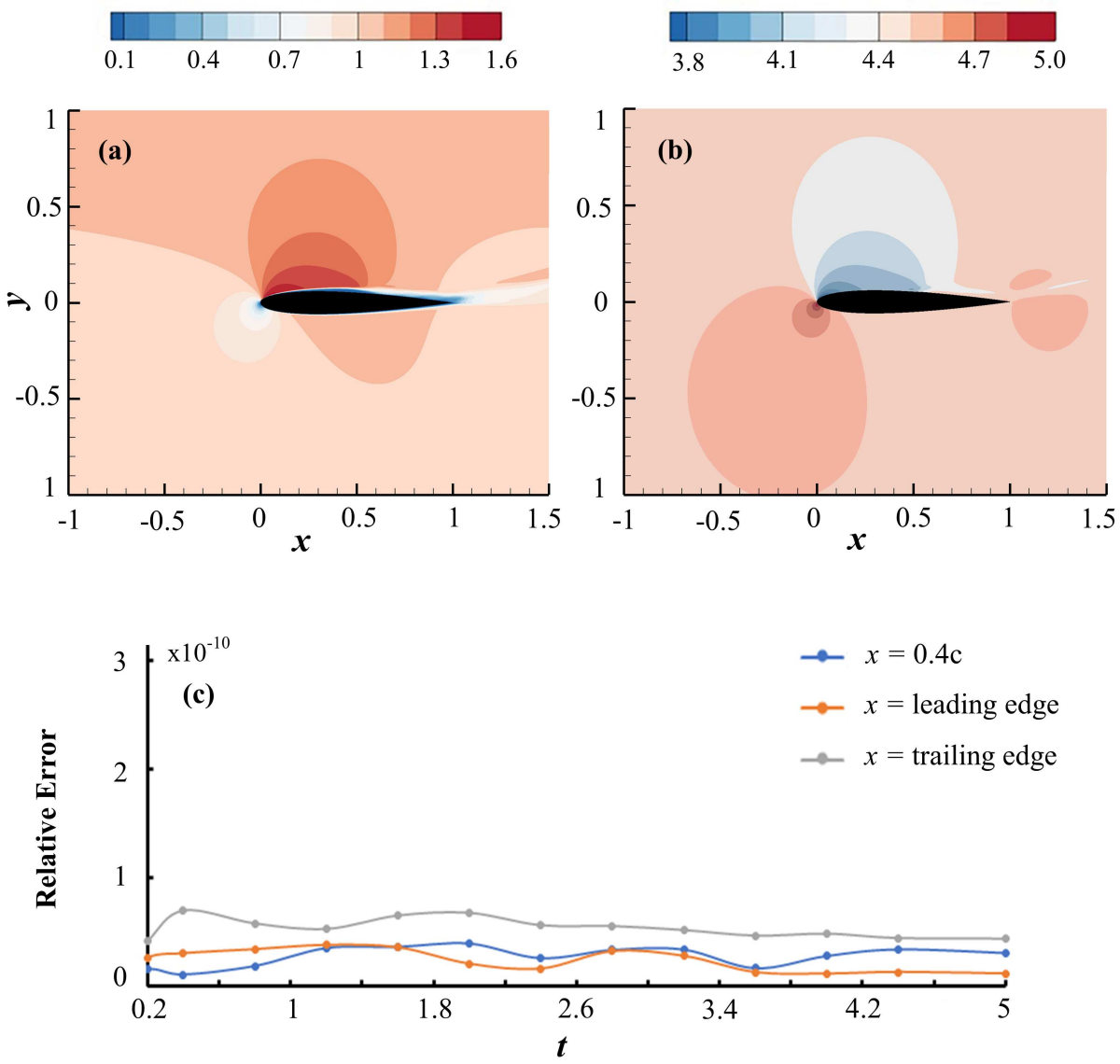

Fig. 1 Steady base flow of *RS* case. (a) Distribution of total velocity. (b) Distribution of pressure. (c) Relative error of pressure from initial flow solution on a streamline very close to airfoil suction surface.

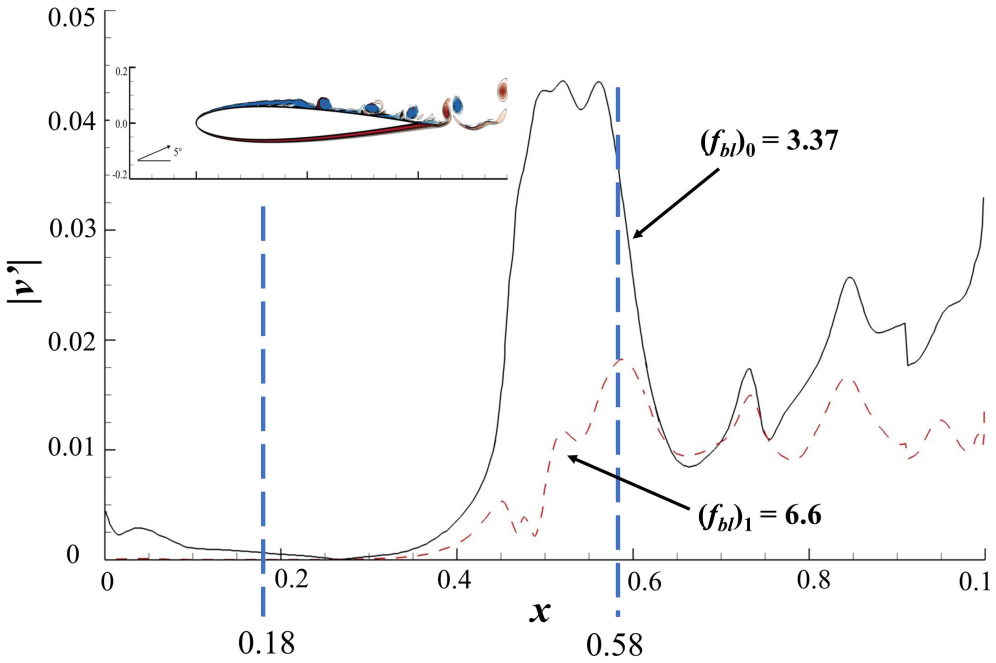

Fig. 2 Spatial growth of flow instability with a snapshot of vorticity distribution. The two blue dashed lines show the extent of separation bubble. The small figure shows snapshot of the flow.

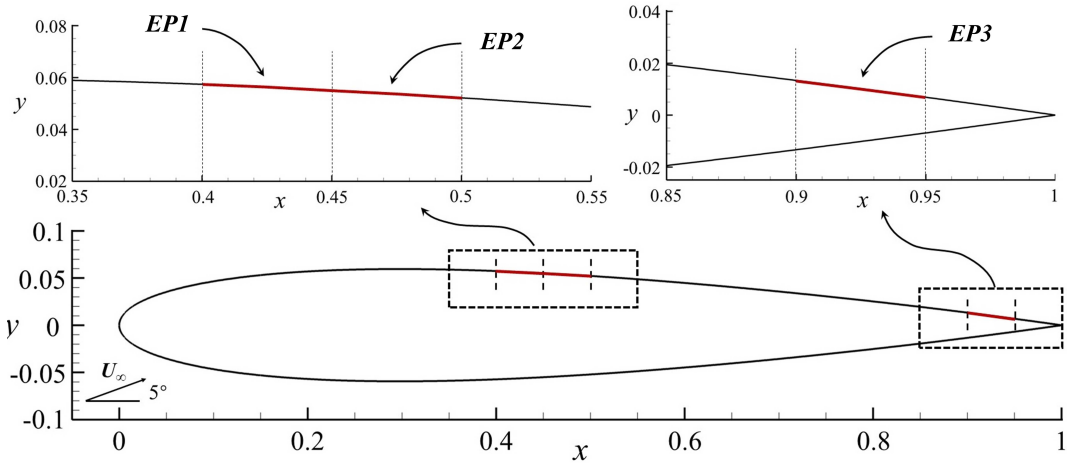

Fig. 3 Schematic sketch of the flow problem and the locations of elastic panels.

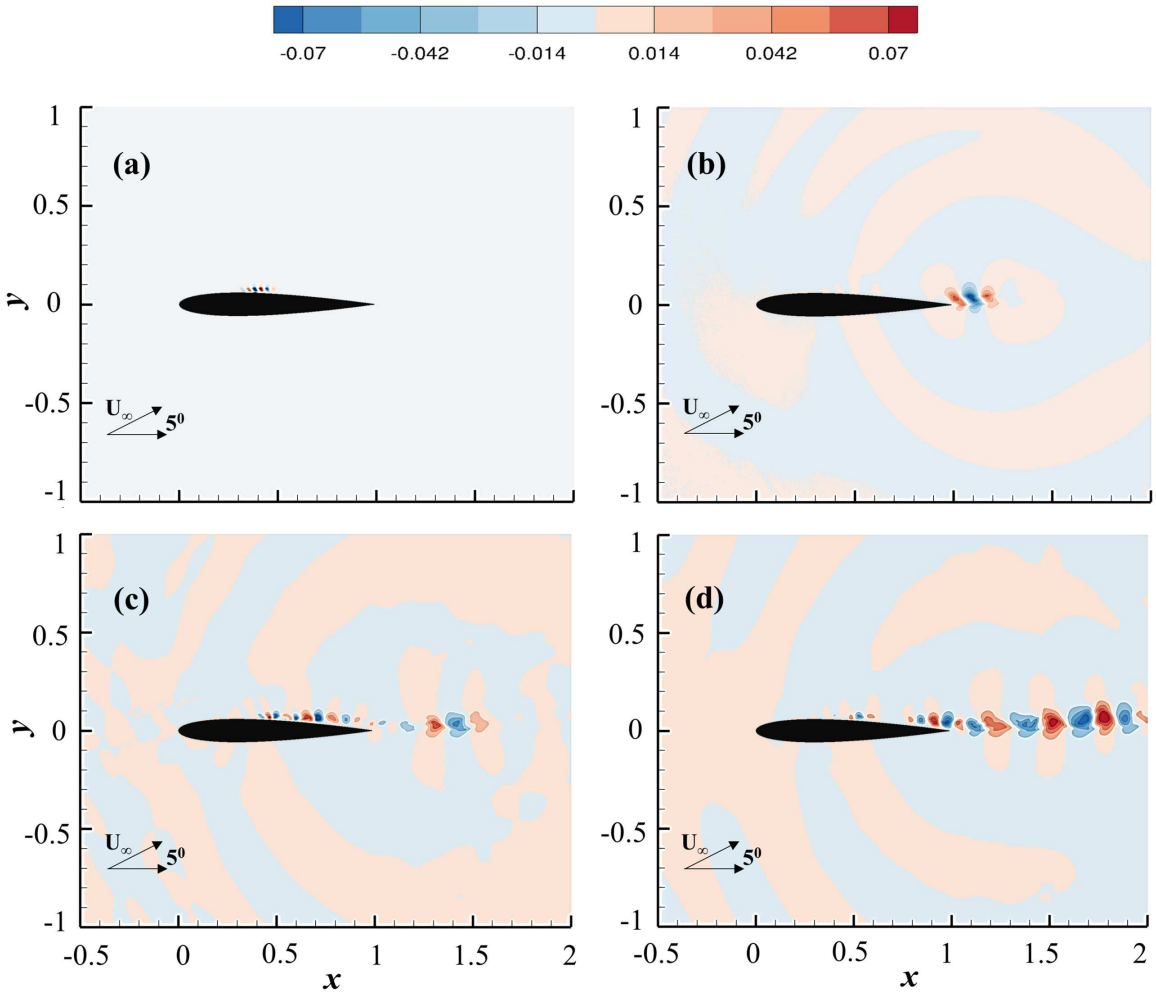

Fig. 4 Evolution of aeroacoustic feedback loop illustrated with transverse velocity fluctuations v'. (a) t=0.5; (b) t=1.0; (c) t=3.5; and (d) t=4.0.

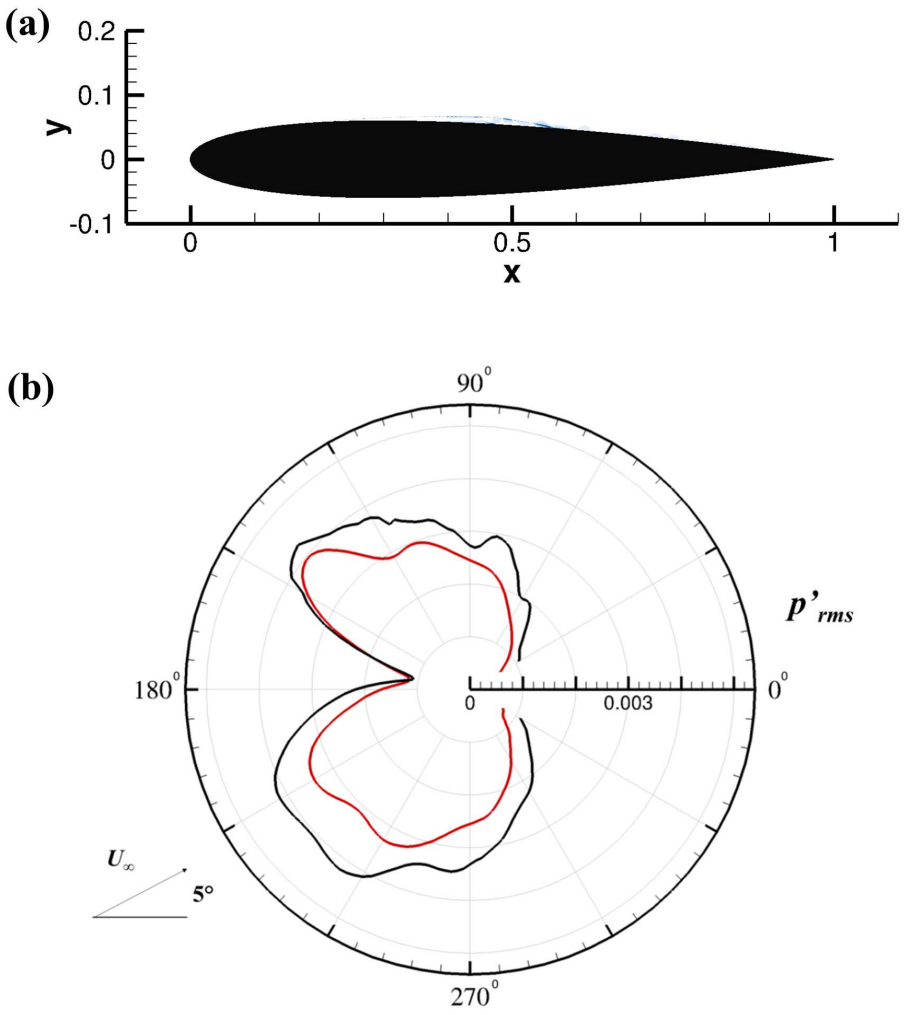

Fig. 5 Relative percentage deviation (= 0.25%) of total velocity between $EP1_{NR}$ and RS base flow determined from DAS solutions. (b) Azimuth distributions of acoustic p'_{rms} for $EP1_{NR}$ case. —-, from perturbation evolution method solution; ——, from DAS solution.

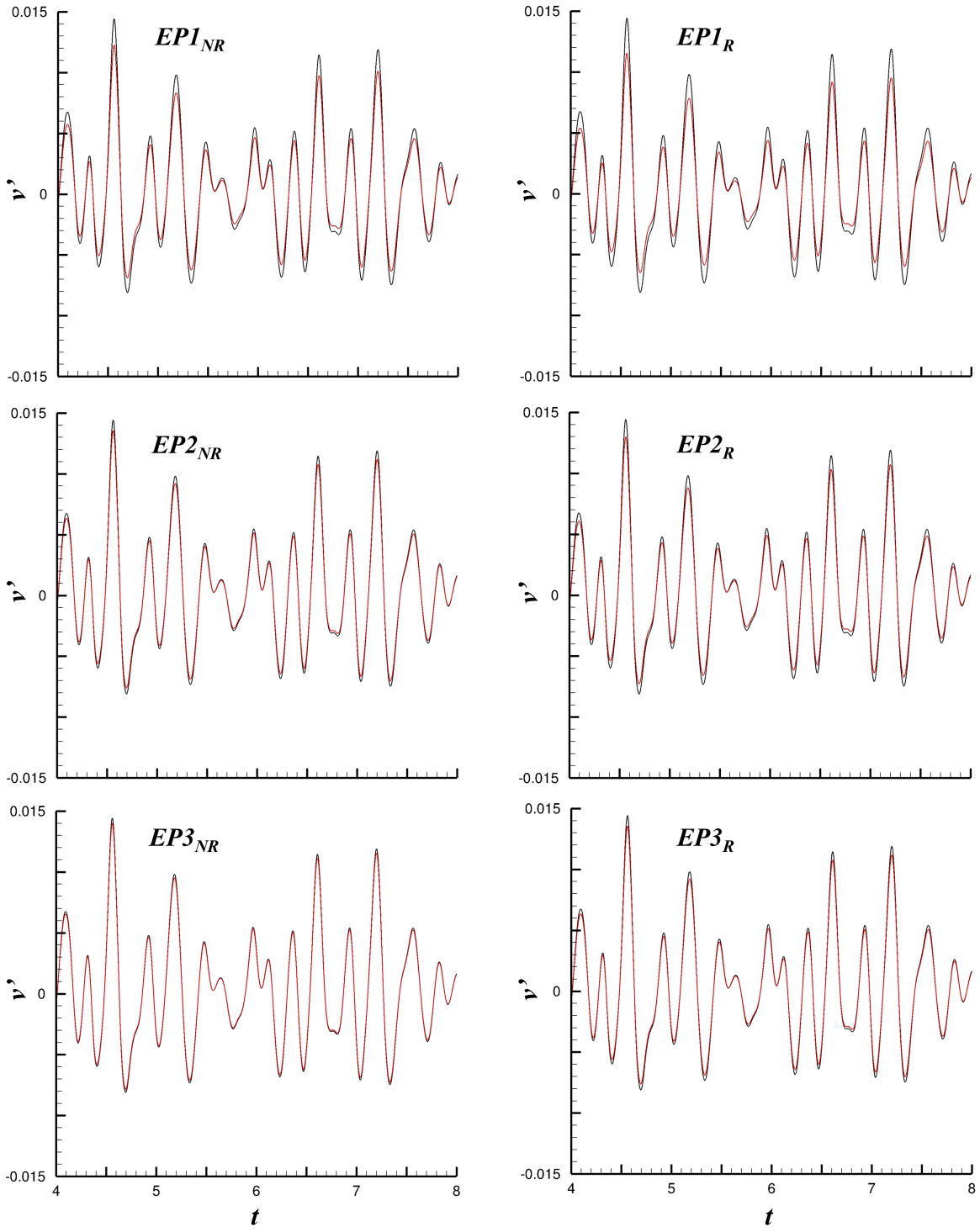

Fig. 6 Effect of elastic panel on flow instability evolution at 99% chord location. First row, *EP*1; second row, *EP*2; third row, *EP*3. ——, with panel; ——, without panel, i.e. *RS*.

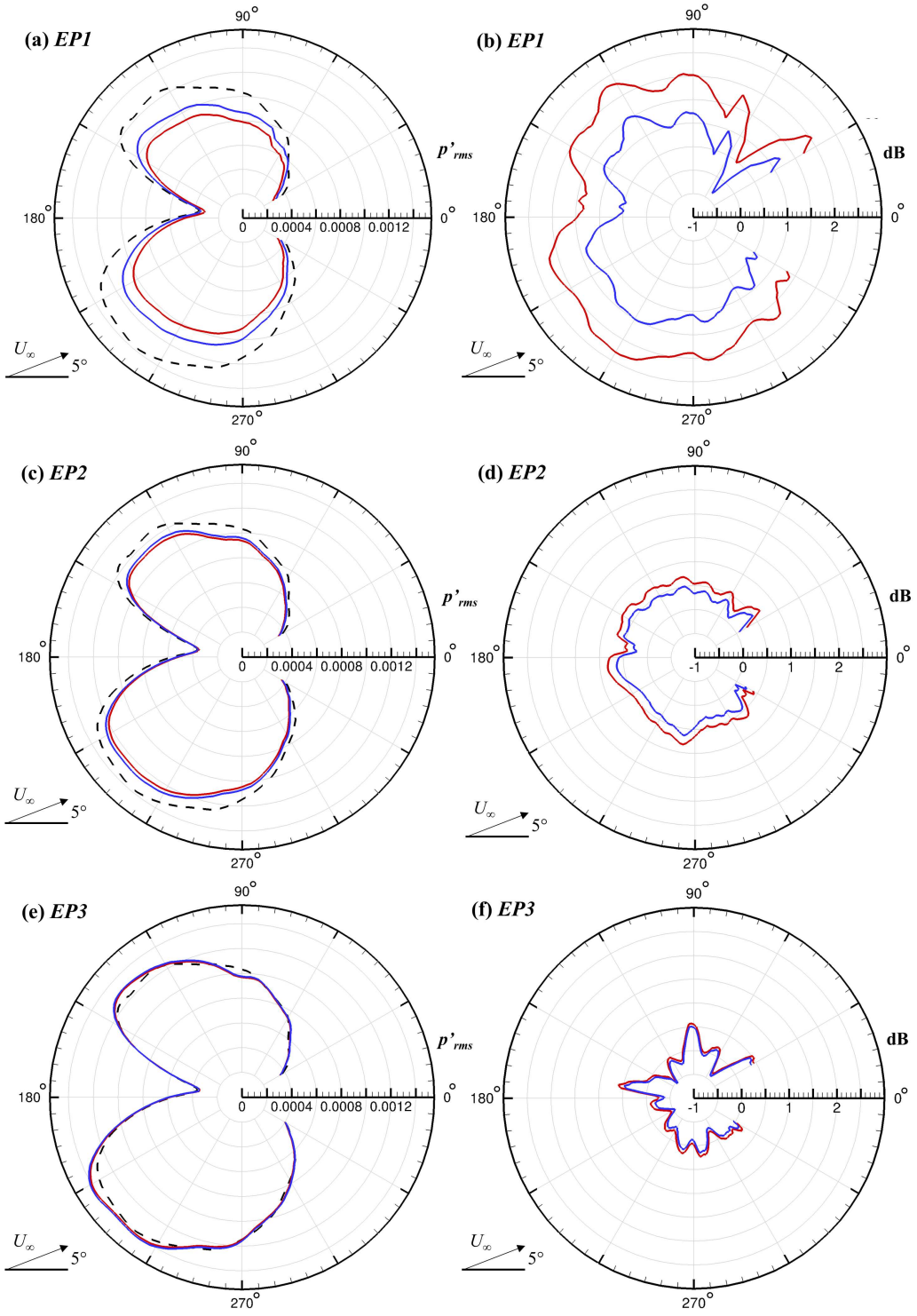

Fig. 7 Effect of elastic panel on noise generation. (a), (c) and (e), distribution of p'_{rms}; (b), (d) and (f) $\Delta SPL_{reduction}$. ——, with resonant panel; ——, with non-resonant panel; - - - -, *RS* cases.

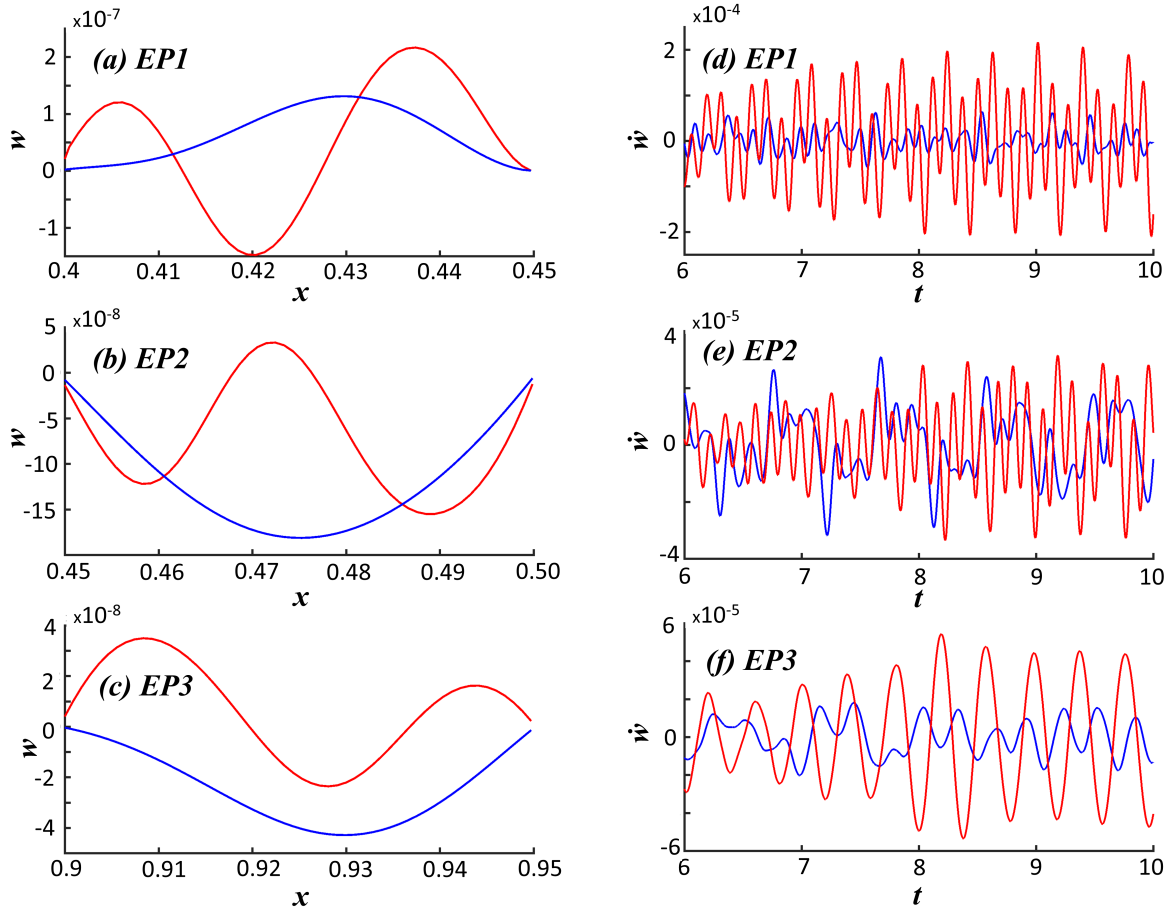

Fig. 8 Vibratory responses of elastic panels. ——, resonant panel; ——, non-resonant panel. Left column, snapshots of vibration modes at $t = 6$. Right column, time histories of displacements at panel center.